J Phys Chem B. Author manuscript; available in PMC 2018 May 11.

Published in final edited form as:

J Phys Chem B. 2017 May 11; 121(18): 4768–4777. doi:10.1021/acs.jpcb.7b02376.

Pyrene-Apelin Conjugation Modulates Fluorophore-and Peptide-Micelle Interactions

Robin E. Patterson[1], **Nathan Weatherbee-Martin**[1], and **Jan K. Rainey**[1,2,*]

[1]Department of Biochemistry & Molecular Biology, Dalhousie University, Halifax, Nova Scotia B3H 4R2 Canada

[2]Department of Chemistry, Dalhousie University, Halifax, Nova Scotia B3H 4R2 Canada

Abstract

Bioactive apelin peptide forms ranging in length from 12 to 55 amino acids bind to and activate the apelin receptor (AR or APJ), a class A G-protein coupled receptor. Apelin-12, -17, and -36 isoforms, named according to length, with an additional N-terminal cysteine residue allowed for regiospecific and efficient conjugation of pyrene-maleimide. Through steady-state fluorescence spectroscopy, the emission properties of pyrene in aqueous buffer were compared to those of the pyrene-apelin conjugates both without and with zwitterionic or anionic micelles. Pyrene photophysics are consistent with an expected partitioning into the hydrophobic micellar cores, while pyrene-apelin conjugation prevented this partitioning. Apelin, conversely, is expected to preferentially interact with anionic micelles; pyrene-apelin conjugates appear to lose preferential interaction. Finally, Förster resonance energy transfer between pyrene and tryptophan residues in the N-terminal tail and first transmembrane segment (the AR55 construct, comprising residues 1–55 of the AR) was consistent with efficient nonspecific pyrene-apelin conjugate binding to micelles rather than direct, specific apelin-AR55 binding. This approach provides a versatile fluorophore conjugation strategy for apelin, particularly valuable given that even a highly hydrophobic fluorophore is not deleterious to peptide behavior in membrane-mimetic micellar systems.

Graphical Abstract

*Corresponding author. Telephone: (902) 494-4632; fax: (902) 494-1355; jan.rainey@dal.ca.

Supporting Information. SDS-PAGE (Figures S1) and HPLC chromatogram (Figure S2) demonstrating Cys-apelin-36 expression, SUMO cleavage and purification. Concentration dependent emission spectra of Py-Cys-apelin-17 in buffer and surfactant micelles (Figure S3).

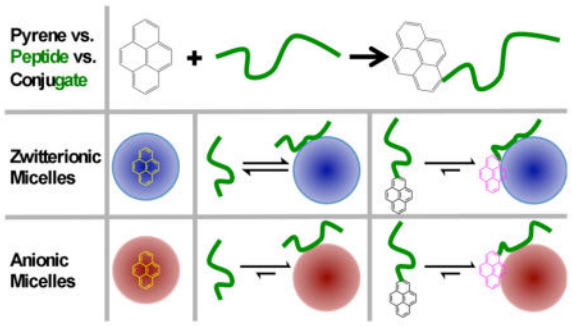

INTRODUCTION

The apelin peptides[1] are cognate ligands to a class A G-protein coupled receptor (GPCR), the apelin receptor[2] (AR; previously known as APJ, or the angiotensin-like receptor 1). Apelin-AR binding and activation has attributed cardiovascular, adipoinsular axis, and nervous system functions.[3] Expanding the complexity of this system, a second peptide ligand to the AR, apela, was recently discovered.[4–5] In line with the membrane catalysis hypothesis,[6] apelin interacts preferentially with and becomes structured upon binding to anionic headgroups vs. to zwitterionic micelles.[7] Interestingly, apela exhibits distinct preferences in micellar interaction relative to apelin.[8]

The bioactive apelin peptides are processed as C-terminal fragments of the 77 amino acid preproapelin precursor protein.[3] Through truncation[9–13] and amino acid substitution[9, 14] studies, it has been shown that the 12 C-terminal amino acids of the preproprotein are required for apelin binding to the AR. Three primary bioactive apelin isoforms have been the focus of pathophysiological and biophysical studies to date: apelin-13, -17 and -36, all named according to the number of C-terminal residues retained. Expanding this family, and correlating with mass spectrometry of colostrum and milk,[15] we recently determined that apelin-55 (previously denoted proapelin, the product of signal peptide removal from preproapelin) is also bioactive.[16] Akin to apelin, apela also may exist in multiple isoforms from 11–32 residues in length,[4–5] although which of these are physiological remains an open question. Two families of peptide ligands with varying lengths and physicochemical properties capable of binding to and activating the same GPCR, with variation in potency and affinity,[3] provide an ideal set of natural permutations for biophysical characterization of ligand-receptor interactions.

Fluorophore conjugation to these peptides is highly appealing as a strategy to study ligand-receptor interactions. In the case of apelin, fluorophore conjugation has been employed in a number of studies by Llorens-Cortes and co-workers to provide a Förster resonance energy transfer (FRET) partner for green fluorescent protein-conjugated AR in evaluation of apelin-AR binding.[17–18] In these studies and others employing fluorescence microscopy to track internalization, conjugation of a variety of fluorophores to the apelin-13 N-terminus have been demonstrated to be non-perturbing to apelin function.[12, 17–20]

Pyrene exhibits high sensitivity to microenvironment polarity. The relative intensities of the pyrene emission bands are modulated, through the Ham effect,[21] as a function of environment.[22] Specifically, pyrene exhibits five distinct emission bands (referred to as bands I-V), with the highest in energy of these (band I) being attributed to the 0–0 vibronic transition with the intensity of this band increasing relative to the other bands as solvent polarity is increased.[22] The ratio of the intensity of band I to that of band III, the so-called *Py* value, is particularly indicative of the polarity of the microenvironment.[23] A *Py* value of less than 1 indicates a highly hydrophobic environment surrounding the pyrene moiety, with increasing *Py* values suggesting increasing hydrophilicity.

Two other features of pyrene photophysics are notable. First, excimer emission by pyrene is also frequently employed as a probe for conformational change or binding, since this phenomenon is contingent upon two pyrene rings being within ~10 Å.[24] Secondly, pyrene acts as a FRET acceptor for tryptophan with a Förster distance of 28 Å.[25] It is thus a strong candidate for evaluation of a fluorophore-conjugated ligand—protein interaction.

Previous studies have used fluorophore conjugation to a single apelin isoform. Building of a series of fluorophore-conjugated apelin peptides would effectively provide a molecular ruler, with increased spacing between the functionally critical C-terminal region of the peptide and the fluorophore provided, by virtue of increasing isoform length. Herein, we have used pyrene as a model fluorophore to develop this strategy both because of its sensitivity to variation in microenvironment and because of its potential to undergo FRET with tryptophan. Given the demonstration that apelin isoforms interact with both zwitterionic and anionic micelles, albeit differently,[7] modulation of this behavior through conjugation of a hydrophobic pyrene is very possible. We therefore focus on a characterization of the behavior of three pyrene-conjugated apelin peptides ranging from 13–37 residues in length (Figure 1A) in the presence of surfactant micelles (Figure 1B). A segment of the AR (AR55, Figure 1C, comprising the first 55 residues of the GPCR[26]) is also employed to test for pyrene-tryptophan FRET. A combination of *Py* values, excimer formation, and FRET between pyrene-conjugated apelin and AR55 imply that fluorophore conjugation promotes efficient apelin-micelle interaction for zwitterionic and anionic micelles without inducing significant fluorophore or peptide penetration into the hydrophobic core of the micelle.

EXPERIMENTAL SECTION

Materials

Acetonitrile, trifluoroacetic acid (TFA), ampicillin, isopropyl β-D-1-thiogalactopyranoside (IPTG), reagents for lysogeny broth (LB) medium, and sodium dodecyl sulfate (SDS) were purchased from Fisher Scientific (Ottawa, ON). Peptide synthesis reagents were obtained from AAPPTec (Louisville, KY). Primers were purchased from Bio Basic Canada (Markham, ON). BL21(DE3) strain *ESCHERICHIA COLI* cells were purchased from Lucigen (Middleton, WI). Dodecylphosphocholine (DPC) was purchased from Anatrace (Maumee, OH). The sodium salt of 1-palmitoyl-2-hydroxy-*Sn*-glycero-3-phospho-(1′-*Rac*-glycerol) (LPPG) was obtained from Avanti Polar Lipids (Alabaster, AL). All other chemicals and solvents were obtained at reagent or high performance liquid chromatography (HPLC) grade from Sigma-Aldrich Canada (Oakville, ON), unless otherwise stated.

Cys-apelin-17 and Cys-apelin-12 synthesis and purification

Solid-phase syntheses of the Cys-apelin-12 and -17 peptides (sequences in Figure 1A) were carried out as reported previously.[27] After lyophilization, each crude peptide product mixture was solubilized in water and resolved using reversed-phase high performance liquid chromatography (RP-HPLC) on a ProStar HPLC equipped with a diode array ultraviolet/visible (UV/Vis) absorbance detector (Varian Canada, Mississauga, ON) through monitoring of absorbance at 210 nm and 280 nm. For analytical purposes, a C_{18} matrix (5 μm particle, 4.6 mm × 250 mm Spirit Peptide column, AAPPTec, Louisville, KY) was employed with a water:acetonitrile (A:B; both containing 0.1% TFA) gradient with B progressing from 2 to 98% in 40 min at 0.8 mL/min flow rate. A preparative C_{18} matrix (5 μm particle, 20 mm × 250 mm Cosmosil column, Nacalai USA, San Diego, CA) employing the same gradient at a flow rate of 8 mL/min was used for purification purposes. Purified product masses were confirmed using positive mode electrospray ionization mass spectrometry (Dalhousie Mass Spectrometry Laboratory, Department of Chemistry, Halifax, NS).

Recombinant Cys-apelin-36 production

A pET-HN vector (gift from Dr. Paul Xiang-Qin Liu, Dalhousie University) with an *E. coli* codon-optimized apelin-36 open reading frame immediately downstream of and in frame with the 6xHis-SUMO gene[16] was modified by insertional mutagenesis (QuikChange Mutagenesis Kit, Agilent Technologies Canada, Mississauga, ON) a codon for cysteine was inserted immediately before that for the N-terminal leucine of apelin-36 (Figure 1A). Mutagenesis was confirmed by DNA sequencing (GENEWIZ, South Plainfield, NJ). BL21(DE3) *E. coli* cells were transformed with this expression plasmid, grown with shaking (200 rpm) for 16 h at 37 °C in 30 mL of LB medium with ampicillin (100 μg/mL) and used to inoculate 2 L of LB medium with ampicillin (100 μg/mL) grown to an optical density at 600 nm of 0.6 at 37 °C with shaking at 200 rpm. Protein expression was induced by IPTG (final concentration 0.5 mM), cells were grown for 3 h at 37 °C, and then harvested by centrifugation (6500g at 4 °C for 20 min). The resulting cell pellet was resuspended in 30 mL lysis buffer (50 mM NaH_2PO_4, 300 mM NaCl, 10 mM imidazole, titrated to pH 8.0 with NaOH) and the cells lysed using a French pressure cell press (American Instrument Company, Silver Springs, MD). The lysate was centrifuged at 15,000g for 30 min at 4 °C.

6xHis-SUMO-Cys-apelin-36 was purified from the supernatant using immobilized metal affinity chromatography with a Ni^{2+}-nitrilotriacetic acid agarose column (Qiagen, Toronto, ON) pre-equilibrated with lysis buffer. The column was washed with 4 column volumes of wash buffer (50 mM NaH_2PO_4, 300 mM NaCl, 20 mM imidazole, pH 8.0), and then the column-bound protein was collected upon addition of elution buffer (50 mM NaH_2PO_4, 300 mM NaCl, 300 mM imidazole, pH 8.0). Column flow-through, wash, and elution fractions were analyzed using SDS-polyacryalamide gel electrophoresis. Elution fractions were combined, and the 6xHis-SUMO expression tag was cleaved from the protein using 200 μL of recombinantly expressed SUMO protease (vector from Addgene, Cambridge, MA) and 1 nM dithiothreitol (DTT), with incubation at room temperature for 4 h. The cleavage product was lyophilized and resuspended in H_2O and Cys-apelin-36 was purified using RP-HPLC (Varian ProStar) on a C_{18} semi-preparative matrix (5 μm particle, 10 mm × 250 mm Cosmosil column) with a water:acetonitrile (A:B; both containing 0.1% TFA) gradient with

B progressing from 2 to 100% in 23 min with a non-linear gradient (20–42.5% B from 0–18 min, 42.5–100% B from 18–23 min) at 3.5 mL/min flow rate. The product mass was confirmed using positive mode electrospray ionization mass spectrometry (Dalhousie Mass Spectrometry Laboratory).

AR55 and AR55 Mutant Production

Employing an *E. coli* codon optimized gene encoding C-terminally His_6-tagged AR55 (amino acid sequence in Figure 1C) cloned into the pEXP5-CT vector, site-directed mutagenesis (QuikChange Mutagenesis Kit) was used to generate independent vectors containing open reading frames encoding for AR55 with single tryptophan residues mutated to phenylalanine at positions W24 and W51 (i.e., W24F-AR55 and W51F-AR55). Mutations were confirmed through sequencing (GENEWIZ). Expression and purification for wildtype and mutant AR55 protein constructs followed our previously detailed inclusion body preparation-based method,[26] with each product mass confirmed using positive mode electrospray ionization mass spectrometry (Dalhousie Mass Spectrometry Laboratory).

Pyrene Conjugation to Apelin Peptides

Purified Cys-apelin-12, -17 or -36 was dissolved in DMF (3 mg/mL) and incubated for 3 h at room temperature with 2–5 molar equivalents of *N*-(1-pyrenyl)maleimide (NPM) dissolved in 100 μL DMF. The reaction of Cys-apelin-36 included 5 mM DTT. Reactions were monitored using RP-HPLC (Varian ProStar) through absorbance at 210 nm and 340 nm using a C_{18} matrix (5 μm particle, 4.6 mm × 250 mm Spirit Peptide column) with a water:acetonitrile (A:B) gradient with B progressing from 2 to 100% in 25 min at 0.8 mL/min flow rate. The reaction mixture was purified on a preparative C_{18} matrix (5 μm particle, 20 mm × 250 mm Cosmosil column) using the same gradient with 8 mL/min flow rate. Product (Py-Cys-apelin-12, -17, or -36) masses were confirmed using positive mode electrospray ionization mass spectrometry (Dalhousie Mass Spectrometry Laboratory).

Emission Spectroscopy Experiments

Stock solutions of each Py-Cys-apelin conjugate were prepared in methanol, with the conjugate content quantified using the Beer-Lambert law by UV/Vis absorbance spectrophotometry (Hewlett Packard 8452A) using a molar extinction coefficient (ε) of 40,000 M^{-1} cm^{-1} at 338 nm for pyrene.[28] Following lyophilization, final samples were prepared through stock solution preparation and dilution to 1 μM peptide and (where appropriate) 100 mM surfactant in 20 mM sodium phosphate buffer containing 60 mM NaCl at pH 7.0, unless otherwise stated. Pyrene control samples were prepared identically for each condition, with 1 μM pyrene substituted for Py-Cys-apelin.

Steady-state fluorescence spectroscopy experiments were carried out using a QuantaMaster-4CW spectrofluorometer (HORIBA Canada, London, ON) controlled using Felix32 software (HORIBA) with data analysis in GraphPad Prism 6 (GraphPad Software, San Diego, CA). Samples were analyzed in 3 mm × 3 mm quartz microcuvettes (Hellma Analytics, Markham, ON) using 150 μL volumes at 37 °C. Both excitation and emission monochromators were set at 4 nm slit widths. The excitation wavelength for all pyrene-labeled samples was 340 nm and emission spectra were recorded from 350 nm – 550 nm

with an integration time of 0.25 nm/s. Each experiment was repeated three times using fresh samples and spectra were averaged and blank subtracted.

For Py-Cys-Apelin—AR55 FRET Experiments, samples containing 20 μM AR55 and 3.5 mM LPPG in 20 mM sodium phosphate buffer with 60 mM NaCl at pH 7 were prepared with Py-Cys-apelin-17 concentration increasing from 0 to 200 μM. Steady-state fluorescence spectroscopy experiments were carried out in an identical manner to that above, except that both excitation and emission monochromators were set at 5 nm slit widths, an excitation wavelength of 295 nm was employed, and emission spectra were recorded from 300 nm to 500 nm (for Py-Cys-apelin-17 concentrations ranging from 0 to 40 μM) or 300 nm to 360 nm (for Py-Cys-apelin-17 concentrations greater than 40 μM) with an integration time of 0.1 nm/s. As with above, each experiment was repeated three times and spectra were averaged.

Py Value and FRET Efficiency Calculation

Py values were calculated for each spectrum using the emission maximum in the 375 nm – 385 nm range (also, in all cases, the overall emission maximum) taken as band I (intensity F_I). The band III intensity (F_{III}) for all spectra was taken at a 10 nm red-shift from band I. After background signal subtraction, the *Py* value was calculated[23] as:

$$Py = F_I / F_{III}. \quad (1)$$

The donor (i.e., tryptophan) emission intensities at each Py-Cys-apelin-17/AR55 titration point (i.e., F_{DA}) and for a given AR55 construct in the absence of Py-Cys-apelin-17 (i.e., F_D) were taken as the intensity at the tryptophan emission maximum (i.e. the emission maximum over the 300 nm – 330 nm range). FRET efficiency (E) was then determined[25] as:

$$E = 1 - \frac{F_{DA}}{F_D}. \quad (2)$$

Py values and FRET efficiencies from each experimental replicate were averaged, with results reported as the mean ± standard error of the mean (SEM).

RESULTS AND DISCUSSION

Pyrene-apelin conjugation

As expected on the basis of native apelin-12 and -17 isoform production,[27] Cys-apelin-12 and -17 were readily produced through solid-phase peptide synthesis and RP-HPLC purified. Recombinant Cys-apelin-36 production as a C-terminal fusion to His_6-SUMO was produced, with efficient immobilized metal affinity chromatography, SUMO protease cleavage, and RP-HPLC purification steps providing a final yield following HPLC of ~2 mg of Cys-apelin-36 per L of LB medium (Figures S1–S2). This method follows from our recombinant production of wildtype human apelin-36.[16]

For all Cys-apelin peptides, NPM conjugation in DMF proceeded efficiently at room temperature (Figure 2), with DMF serving as an excellent co-solvent both for NPM and the apelin peptides. A stoichiometry of 2:1 to 5:1 (NPM:apelin) allowed for robust conjugation, a significantly reduced (although not unprecedented[29]) stoichiometry relative to typical protocols.[30–31] In the case of Cys-apelin-36, addition of DTT was required, presumably to reduce disulfide-linked dimers and allow for NPM conjugation. Thus, the addition of a cysteine residue at the N-terminus of three different isoforms of apelin allows for efficient and specific labeling at >95% efficiency (Figure 2) with a fluorescent probe.

This technique can be modified to suit the particular experiment of interest. Because of the versatility of DMF as a solvent, the relatively low stoichiometric excess required vs. typical literature protocols, and the variety of fluorescent probes with maleimide linkers that are commercially available, it is likely that this method could be used for any number of different fluorescent dyes, making it possible to conjugate a dye with specific spectral properties tailored to the desired experiment. It would also be feasible to synthesize or mutate apelin isoforms with a cysteine residue in different positions in the sequence to probe other areas of the peptide. In particular, probes may be valuable in close proximity to the RPRL motif or at the C-terminus, segments within apelin-13 that have been shown to be sensitive to amino acid substitution[9, 14] and which we have previously shown to be relatively conformationally restricted.[7, 27]

Emission spectroscopy

To provide a reference for pyrene behavior, steady-state emission spectroscopy experiments were carried out using pyrene in buffer and in each micellar environment (Figure 3). Surfactant concentrations were maintained at 100 mM, considerably exceeding the reported critical micelle concentrations (CMCs) of ~4 mM,[32] ~1.1 mM,[33] and ~0.02 mM[33] for SDS, DPC, and LPPG, respectively. Based upon reported aggregation numbers of 59–68 for SDS,[34] 75–80 for DPC,[35] and 125 at low salt[36] to 160–170 at 150 mM NaCl[35] for LPPG, micelles are in very high stoichiometric excess relative to the 1 μM fluorophore concentration used in these experiments. In all environments, pyrene exhibits the expected[37] five bands between ~370 and 430 nm.

Notably, pyrene emission increases in intensity in each micellar environment relative to buffer (Figure 3). Correspondingly, at the pyrene:micelle stoichiometries employed, no evidence of excimer formation is seen (i.e., no significant emission intensity was observed above 480 nm). Increased pyrene emission intensity in the presence of micelles is hence consistent with literature behavior in SDS micelles of bound vs. free pyrene monomers well above the critical micelle concentration.[38] Beyond a general increase in intensity, pyrene also exhibits an expected[22, 39] increase in intensity of bands II-V relative to band I. This photophysical behavior is consistent with partitioning into the hydrophobic core of the micelle.[23, 39]

Fluorescence emission spectra were acquired for all three pyrene-conjugated isoforms of apelin (Py-Cys-apelin-12, -17, and -36; 1 μM) in buffer both without surfactant and in the presence of SDS, DPC and LPPG micelles (100 mM surfactant concentration; Figure 4). Notably, in buffer, excimer formation was observed in Py-Cys-apelin-36; conversely, Py-

Cys-apelin-12 and Py-Cys-apelin-17 exhibited no excimer bands (Figure 4). Free pyrene also exhibited no excimer at 1 μM concentration (Figure 3). Given an identical pyrene concentration of 1 μM for each of these samples, this implies a drive for self-association of the sparingly soluble[40] pyrene in buffer that is modulated by the nature of the conjugated peptide.

To further examine the dependence of pyrene self-association upon apelin isoform, emission properties of Py-Cys-apelin-12 and -17 were investigated in a concentration dependent manner. With Py-Cys-apelin-17, excimer bands were not enhanced over 1–10 μM of peptide-conjugate in either buffer or micellar solution, although slight enhancement of lower energy emission band intensity relative to band I was observed in DPC and LPPG micelles (Figure S3). With Py-Cys-apelin-12, conversely, excimer formation was enhanced as a function of peptide-conjugate concentration, leading to an excimer emission intensity almost equivalent to that of monomeric band I upon increase to 11 μM Py-Cys-apelin-12 (Figure 5). The caveat should be noted that these data were acquired in sub-CMC (1 mM) SDS, rather than in buffer. In the case of Py-Cys-apelin-36, where excimer emission is observed in buffer, the region proximal to the conjugation site is relatively hydrophobic (Figure 1A). It is therefore possible that self-association is driven by hydrophobicity, which is counteracted through micellar interactions. This corresponds to the solubility of free pyrene in buffer, with the 1 μM employed being near maximal.[40] With Py-Cys-apelin-17, the entire isoform is relatively hydrophilic and the pyrene conjugation site is proximal to a highly cationic segment (Figure 1A). This appears to be sufficient to keep the pyrene functionality soluble as a monomer in aqueous solution. Finally, with apelin-12, although the peptide itself is relatively hydrophilic (Figure 1A), it appears that this is insufficient to counteract the propensity for aqueous environment-induced pyrene self-association but sufficient to prevent the precipitation expected[40] for free pyrene at similar concentrations.

Upon addition of surfactant micelles, regardless of the micelle type and apelin isoform length, evidence of excimer formation was not observed. Going beyond the simple micelle to peptide stoichiometry argument above, this provides further evidence that the micelle-to-peptide ratio is sufficient to ensure at most one peptide per micelle. The presence of surfactant monomers in solution at the CMC is also not a contributing factor, as tested with Py-Cys-apelin-12 and SDS at ratios of up to 1:100 peptide-conjugate:surfactant (Figure 5). In all, the loss of excimer in the presence of all micelles also implies that there is not a significant driving force for the amphipathic Py-Cys-apelin molecules to self-associate into micelles in solution; rather, association with surfactant micelles is favored.

Excluding isoform-dependent excimer formation in buffer, the same general trends were observed for each sample type across all three peptides. First, emission intensity increased with the addition of each of the three micelles relative to buffer. Intensity was observed to increase from buffer to SDS to LPPG and DPC. In the case of Py-Cys-apelin-12, a distinct increase in emission intensity from LPPG to DPC was observed, while each of the longer Py-Cys-apelin isoforms in LPPG and DPC exhibited practically indistinguishable emission intensities. One mechanism for increased intensity would be loss of monomeric emission quenching by excimer formation for the shorter apelin isoforms. However, this phenomenon was observed for all three isoforms of pyrene-labelled apelin (as well as the two control

samples), implying that the primary source of increased intensity is attributable[38] to pyrene-micelle binding.

Secondly, similar emission spectrum red-shift behavior was observed with each Py-Cys-apelin isoform. The emission spectra for all three apelin isoforms were significantly red-shifted compared to pyrene, with additional red-shifts of small magnitudes as a function of increasing apelin isoform length (Figure 4; Table 1). Modified photophysics as a result of deviating from a symmetric pyrene to an asymmetric Py-Cys-apelin species is a likely source of the red-shifts observed relative to pyrene.[41] The differences observed between the Py-Cys-apelin isoforms, conversely, may arise from the differences in propensity for excimer formation.[38]

Pyrene and each of the Py-Cys-apelin isoforms also exhibited a similar red shift behavior between buffer and the surfactant micelle conditions. This, again, is consistent with pyrene monomer emission behavior in other micelles.[38] In general, SDS produced a red-shift of lesser magnitude than either DPC or LPPG. In comparison to the difference in behavior between the apelin-conjugated vs. control molecules, these shifts are extremely minimal (Table 1).

Microenvironment assessment

In the case of pyrene, a clear increase in emission intensity and modulation of band pattern is apparent from buffer to SDS to LPPG to DPC (Figure 3). The ratio of the intensities of band I to band III gives the so-called *Py* value (eq. 1). *Py* values were calculated for each condition (Table 2), with pyrene exhibiting a decrease from ~1.5 in buffer to ~1.2 in DPC and ~1.0 in SDS and LPPG. These values are similar to reported values for pyrene in water[39] (with the caveat that higher values have also been reported[23]), phosphatidylcholine bilayers in the liquid-disordered phase,[42] and SDS micelles[39, 43] (again, with variations in the literature[38]).

The general trend observed for pyrene corresponds to a decrease in the effective dielectric constant of the microenvironment[23, 39] in the move from buffer to zwitterionic DPC micelles to anionic LPPG and SDS micelles. This is consistent with strongly favored partitioning of the pyrene into the hydrophobic micelle core in each instance. Given this partitioning, which has been extensively described in the literature (e.g., [38]), the distinct *Py* value for DPC micelles relative to the anionic micelles may stem either from differences in the headgroups or in the micellar core (Figure 1B). The dipole moment of DPC is calculated to be ~15 D[44] (all dipole moments reported as tabulated in the Pitt Quantum Repository using the MP6 semiempirical quantum chemical model[45] as implemented in MOPAC), whereas that of SDS is expected to be much smaller at ~4.7 D.[46] The molecule, [(1*R*)-1-[[[(2*S*)-2,3-dihydroxypropoxy]-hydroxy-phosphoryl]oxymethyl]-2-hexadecanoyloxy-ethyl] (*z*)-octadec-11-enoate has the same headgroup as LPPG but two alkyl chains instead of one is calculated to have a dipole moment of ~5.3 D,[47] highly comparable to that of SDS. In all instances, the dipole moment is primarily due to the headgroup, rather than the alkyl tailgroup(s) of the molecule. Hence, it seems likely that the elevated *Py* of pyrene in DPC micelles relative to the anionic micelles arises from the properties of the headgroup. An alternative hypothesis, based on the potential for hydrophobic cores of micelles allow for

significant water penetration (e.g., [48]), would be partitioning of a higher mole fraction of water into the DPC micelle core relative to either SDS or LPPG.

All three Py-Cys-apelin isoforms in sodium phosphate buffer in the absence of surfactant exhibited *Py* values of ~1.4 (Table 2), similar to the *Py* value of pyrene in buffer at 1.49. Upon addition of SDS micelles, the *Py* values for both Py-Cys-apelin-12 and -36 increased to ~1.6 while that for Py-Cys-apelin-17 increased to ~1.8. The *Py* values for all three isoforms in the presence of both zwitterionic DPC micelles and anionic LPPG micelles were of similar magnitude, at ~1.8. As observed for Py-Cys-apelin-17, this behavior is fully consistent over peptide concentrations of 1–10 μM (Figure S3). The general trend for all three isoforms of pyrene-labelled apelin is a significant increase in *Py* value with the addition of anionic or zwitterionic surfactant micelles. Notably, this is opposite to the trend observed with pyrene.

We previously showed that apelin-12 and -17 bind favorably to anionic SDS and LPPG micelles, and show a weaker, and likely more transient, interaction with zwitterionic DPC micelles.[7] In the present study, it is not possible to distinguish between the types of interactions taking place with anionic vs. zwitterionic micelles. The slightly greater *Py* values observed in DPC samples with both Py-Cys-apelin-12 and -36 relative to those observed in anionic micelle samples cannot be directly related to propensity for binding. The *Py* value is a function of the interaction between pyrene and the surrounding environment and is influenced by several factors, including hydrogen bonding and dipole moment of the solute and solvent.[37] Of all of these factors, it has been suggested that the dipole moment of the surrounding molecules influences *Py* most prevalently.[39] Hence, the increased *Py* value may be attributable to the much greater dipole moment of ~15 D for DPC vs. ~5 D for either of the anionic surfactants. Therefore, even if the binding between the peptide and micelle is weaker or less prevalent with DPC, the dipole-dipole interaction would be stronger, resulting in a greater *Py* value. As noted above, the potential confounding effect of differences in water partitioning as a function of headgroup[48] also cannot be ruled out.

In comparing the behavior of the pyrene-conjugated apelin peptides to pyrene, it is clear that the *Py* values exhibit opposite behavior in micelles vs. buffer. With pyrene itself, the decreased *Py* value in micellar solution is consistent with fluorophore partitioning into the hydrophobic core of the micelle, albeit with some variation in *Py* as a function of surfactant headgroup indicative of relative proximity to the polar headgroups. The observation of exactly the opposite trend for all three of the Py-Cys-apelin isoforms implies that the pyrenyl group is not partitioning into the micelle core; instead, its behavior in all isoforms is consistent with a close proximity to the polar headgroups accentuating band III at the expense of band I. The N-terminal regions of both apelin-17 and -12 are predominantly composed of basic residues (Figure 1A), providing a reasonable barrier for partitioning of the pyrenyl-maleimide-Cys group to the micelle interior. However, this behavior is notably retained even for Py-Cys-apelin-36, where the N-terminal residues of the isoform are a hydrophobic Leu-Val sequence (Figure 1A). This is consistent with our structural and biophysical characterization of apelin-17 binding to micelles, where no evidence of peptide partitioning to the micelle interior was observable through paramagnetic relaxation enhancement-based NMR experiments even for hydrophobic segments of the peptide.[7]

Importantly, therefore, there is a stronger driving force for the peptide to remain in a polar environment than to permit the otherwise spontaneous partitioning of the pyrenyl group into the hydrophobic micelle interior.

It should be noted that one argument for this difference in behavior could be the increased polarity introduced in proximity to the pyrene through the maleimide functionality. Contrary to this hypothesis, pyrene-maleimide-conjugated α-synuclein exhibited a Ca^{2+}-dependent decrease in *Py* value indicative of partitioning into a hydrophobic microenvironment in vesicles.[49] The lack of hydrophobic partitioning by the pyrenyl group of the Py-Cys-apelin species, therefore, appears to be indicative of the fundamental properties of the apelin peptides themselves, rather than of the pyrene-maleimide group.

Py-Cys-apelin—Trp FRET in micelles

The AR55 region comprising the N-terminal tail and first transmembrane segment has been structurally characterized in DPC,[26] SDS (PDB entry 2LOT), and LPPG micelles (PDB entry 2LOV). A pair of acidic residues (E20 and D23; colored red, Figure 1C) in the AR N-terminal tail has been implicated in apelin-AR binding through mutagenesis,[50] with this region exhibiting structural convergence to provide an anionic patch.[26] AR55 has two Trp residues, located in such a manner to place them proximal to each face of the membrane (colored blue, Figure 1C).[26] Emission spectra of each AR55 sample in the absence of Py-Cys-apelin-17 exhibit similar emission maxima (~320–321 nm; Figure 6), implying that relatively similar environments are experienced by each tryptophan in the wild-type AR55. A blue-shift of this magnitude, relative to the anticipated ~340–350 nm for a tryptophan sidechain exposed to water, would be consistent with both W24 and W51 being found in relatively non-polar environments (e.g., in proximity to the micellar headgroup[51] or buried in the micellar core[52]).

Notably, the AR55 emission intensity is lower than would be expected from summing the contributions of the individual mutants. The kinked nature of the AR55 transmembrane segment[26] including in LPPG (PDB entry 2LOV), alongside the relative plasticity expected of a micellar environment,[53] mean that motion of the two structured micelle-embedded helical segments may undergo significant conformational sampling. In the LPPG NMR ensemble for AR55, the average W24–W51 sidechain Nε1 distance is 35 ± 4 Å. However, in one ensemble member, this approach is as close as 19 Å. Trp-Trp homotransfer has been reported for distances on this order,[54] for this interaction. This phenomenon extending just beyond the upper-end R_0 would, in turn, lead to apparent Trp quenching in the AR55 construct containing two Trp residues vs. the single-Trp mutants. Although other mechanisms cannot be ruled out, this seems a plausible source of the less pronounced increase in intensity observed for AR55 relative to the two single-Trp mutants.

Pyrene-Trp FRET, with an R_0 of 28 Å,[25] provides an alternative means to test for membrane binding by Py-Cys-apelin peptides. Using LPPG micelles, the ability of Py-Cys-apelin-17 to act as a FRET donor for Trp residue(s) in AR55 was tested both for the wildtype protein and for two single-Trp AR55 mutants, W24F and W51F. LPPG was chosen both because of its low CMC (~0.02 mM[33]) and because it is largest of the three micelles employed herein, with a small-angle X-ray scattering profile consistent with an oblate ellipsoid of axial dimensions

of 19–20 Å for the minor semi-axis and 28.4–29.4 Å for the major semi-axis.[55] The former property is beneficial for minimization of free surfactant in the FRET samples while the latter property provides the largest potential for distance-based contrast between FRET due to specific apelin-AR binding and non-specific apelin-micelle binding.

For all FRET experiments, AR55 was maintained at constant concentration (20 μM) with LPPG at a concentration (3.5 mM) providing 1.1–1.5 stoichiometric equivalents of micelles per AR55 based upon the reported aggregation number range of 125–170.[35–36] Py-Cys-apelin-17 was titrated into these samples at a stoichiometry ranging from 0.05:1 to 10:1 relative to AR55. Wildtype and both mutant AR55 proteins exhibited substantial FRET, as evidenced by Py-Cys-apelin-17 concentration-dependent quenching of AR55 Trp fluorescence (Figure 6).

FRET efficiencies (eq. 2) and *Py* values (eq. 1) were determined at each apelin:AR55 stoichiometry (Table 3). In each case, *Py* values converged to ~1.9, falling within one standard deviation of the *Py* value observed for Py-Cys-apelin-17 in LPPG micelles. At the lowest Py-Cys-apelin-17 concentration of 1 μM, *Py* value determination was likely convoluted by Trp emission; at higher ligand concentrations, the relative contribution of Trp emission in the region at 385 nm and above becomes negligible. In short, the ensemble-averaged environment experienced by the pyrene probe is not significantly perturbed in the presence of AR55 relative to that without. Tryptophan, conversely, exhibited a blue shift as a function of FRET-based quenching (Table 3).

FRET efficiency in each instance increased as a function of Py-Cys-apelin-17 concentration to a plateau, with an E of 0.5 achieved between 1 and 2 equivalents of ligand relative to AR55/micelle in each instance. In each case, the E observed is reflective of the ensemble-averaged population of Trp residues as a linear combination of the proportion quenched by FRET and of that not quenched. FRET may occur either by Py-Cys-apelin-17 being brought into proximity with AR55 through non-specific apelin-micelle binding, apelin-AR55 binding, or a combination of both. Based upon our ensemble of AR55 structures in LPPG micelles, the average W24–W51 sidechain Nε1 distance is 35 ± 4 Å. If apelin were tightly binding specifically to the E20/D23 region of AR55, the typical distance of 8.5 Å from either the E20 or D23 sidechain carboxylates to the W24 Nε1 imply a pyrene-Trp distance always shorter than R_0. Alternatively, the structural ensemble imply that the average distance to W51 from either of these acidic sidechains would be ~25–29 Å longer than to W24. Hence, given the sterically necessary extension of the N-terminal Py-maleimide-Cys further from the acidic residues (given a lack of micelle-embedding implied by *Py* values), a situation of strictly apelin-AR55 binding would produce pyrene-W51 distances likely to typically be longer than R_0.

In the context of these structurally-imposed distances, if apelin were specifically binding to AR55, significantly more efficient FRET would be expected in the W51F mutant than in the W24F mutant. The similar FRET behavior of both mutants, therefore, implies that this is likely due primarily to apelin-micelle binding. This is further upheld by the wildtype AR55, with both Trp residues, where there is not a substantial difference in the FRET behavior relative to the single mutants implying that FRET is arising from a non-specific apelin-

micelle interaction. The FRET process, therefore, should have a corresponding dependence upon apelin-micelle binding affinity and stoichiometry rather than upon apelin-AR55 affinity and stoichiometry.

Conclusions

Combining all of these findings, pyrene-apelin conjugation modulates the behavior of both the hydrophobic fluorophore and the cationic peptide. Incorporation of an N-terminal cysteine provided a robust means of pyrene conjugation to bioactive apelin isoforms from 12 to 36 residues in length. Of all of these isoforms, only the Py-Cys-apelin-36 conjugate showed evidence of pyrene self-association and corresponding excimer formation under typical experimental conditions. At higher peptide conjugate concentrations, Py-Cys-apelin-12 also exhibited excimer formation in excess sub-CMC SDS. Upon incubation with micelles, excimer formation was lost, demonstrating greater favorability of peptide conjugate-micelle interactions vs. pyrene-pyrene self-association. Unlike the pyrene controls, where partitioning into the hydrophobic micellar core is implied, Py-Cys-apelin conjugates exhibited pyrene photophysics consistent with micellar binding and an increase in the dielectric of the environment – likely through close proximity to the charged micellar headgroup. This also contrasts with unconjugated apelin isoforms, where binding to anionic over zwitterionic micelles is preferred, given that pyrene emission spectra of the peptide conjugates were consistent with efficient binding in all cases. Using Py-Cys-apelin-17 and the anionic LPPG micelles as a test case, pyrene-tryptophan FRET was employed with the AR55 segment containing two tryptophan residues as well as two AR55 single-tryptophan mutants. In all instances, efficient tryptophan quenching was observed as a function of Py-Cys-apelin-17 concentration. Based upon the expected micellar dimensions and tryptophan positioning inferred from NMR structural studies, this is indicative of efficient apelin conjugate-micelle binding rather than specific apelin-AR55 interaction. For future application, maleimide cysteine conjugation provides a versatile approach to tag apelin isoforms with the extremely valuable potential to introduce a variable-length peptidic spacer between the C-terminal motifs involved in AR binding and activation and the tag.

Acknowledgments

Thanks to Bruce Stewart for technical support; Dr. Pascaline Ngweniform for preliminary experiments employing pyrene-apelin conjugates; Nigel Chapman for SUMO protease production; and, to Nigel Chapman, Aditya Pandey, and Kyungsoo Shin for helpful discussions. This work was supported by a Canadian Institutes of Health Research (CIHR) Operating Grant (MOP-111138); Strategic Cooperative Education Initiative funding from Nova Scotia Economic and Rural Development and Tourism; and, key infrastructure from the Natural Sciences and Engineering Research Council of Canada, Dalhousie Medical Research Foundation, and Canadian Foundation for Innovation. JKR is supported by a CIHR New Investigator Award.

References

1. Tatemoto K, Hosoya M, Habata Y, Fujii R, Kakegawa T, Zou MX, Kawamata Y, Fukusumi S, Hinuma S, Kitada C, et al. Isolation and characterization of a novel endogenous peptide ligand for the human APJ receptor. Biochem Biophys Res Commun. 1998; 251:471–476. [PubMed: 9792798]
2. O'Dowd BF, Heiber M, Chan A, Heng HH, Tsui LC, Kennedy JL, Shi X, Petronis A, George SR, Nguyen T. A human gene that shows identity with the gene encoding the angiotensin receptor is located on chromosome 11. Gene. 1993; 136:355–360. [PubMed: 8294032]

3. Chapman NA, Dupre DJ, Rainey JK. The apelin receptor: Physiology, pathology, cell signalling, and ligand modulation of a peptide-activated class A GPCR. Biochem Cell Biol. 2014; 92:431–440. [PubMed: 25275559]
4. Chng SC, Ho L, Tian J, Reversade B. ELABELA: A hormone essential for heart development signals via the apelin receptor. Dev Cell. 2013; 27:672–680. [PubMed: 24316148]
5. Pauli A, Norris ML, Valen E, Chew GL, Gagnon JA, Zimmerman S, Mitchell A, Ma J, Dubrulle J, Reyon D, et al. Toddler: An embryonic signal that promotes cell movement via Apelin receptors. Science. 2014; 343:746.
6. Sargent DF, Schwyzer R. Membrane lipid phase as catalyst for peptide-receptor interactions. Proc Natl Acad Sci U S A. 1986; 83:5774–5778. [PubMed: 2874556]
7. Langelaan DN, Rainey JK. Headgroup-dependent membrane catalysis of apelin-receptor interactions is likely. J Phys Chem B. 2009; 113:10465–10471. [PubMed: 19708686]
8. Huang SK, Shin K, Sarker M, Rainey JK. Apela exhibits isoform- and headgroup-dependent modulation of micelle binding, peptide conformation and dynamics. Biochim Biophys Acta. 2017; 1859:767–778. [PubMed: 28132903]
9. Medhurst AD, Jennings CA, Robbins MJ, Davis RP, Ellis C, Winborn KY, Lawrie KW, Hervieu G, Riley G, Bolaky JE, et al. Pharmacological and immunohistochemical characterization of the APJ receptor and its endogenous ligand apelin. J Neurochem. 2003; 84:1162–1172. [PubMed: 12603839]
10. De Mota N, Lenkei Z, Llorens-Cortes C. Cloning, pharmacological characterization and brain distribution of the rat apelin receptor. Neuroendocrinology. 2000; 72:400–407. [PubMed: 11146423]
11. Tatemoto K, Takayama K, Zou MX, Kumaki I, Zhang W, Kumano K, Fujimiya M. The novel peptide apelin lowers blood pressure via a nitric oxide-dependent mechanism. Regul Pept. 2001; 99:87–92. [PubMed: 11384769]
12. El Messari S, Iturrioz X, Fassot C, De Mota N, Roesch D, Llorens-Cortes C. Functional dissociation of apelin receptor signaling and endocytosis: Implications for the effects of apelin on arterial blood pressure. J Neurochem. 2004; 90:1290–1301. [PubMed: 15341513]
13. Ceraudo E, Galanth C, Carpentier E, Banegas-Font I, Schonegge AM, Alvear-Perez R, Iturrioz X, Bouvier M, Llorens-Cortes C. Biased signaling favoring G_i over β-arrestin promoted by an apelin fragment lacking the C-terminal phenylalanine. J Biol Chem. 2014; 289:24599–24610. [PubMed: 25012663]
14. Fan X, Zhou N, Zhang X, Mukhtar M, Lu Z, Fang J, DuBois GC, Pomerantz RJ. Structural and functional study of the apelin-13 peptide, an endogenous ligand of the HIV-1 coreceptor, APJ. Biochemistry. 2003; 42:10163–10168. [PubMed: 12939143]
15. Mesmin C, Fenaille F, Becher F, Tabet JC, Ezan E. Identification and characterization of apelin peptides in bovine colostrum and milk by liquid chromatography-mass spectrometry. J Proteome Res. 2011; 10:5222–5231. [PubMed: 21939284]
16. Shin K, Chapman NA, Sarker M, Kenward KA, Huang SK, Weatherbee-Martin N, Pandey A, Dupré DJ, Rainey JK. Bioactivity of the putative apelin proprotein expands the repertoire of apelin receptor ligands. Biochim Biophys Acta. 2017 Revision requested.
17. Iturrioz X, Gerbier R, Leroux V, Alvear-Perez R, Maigret B, Llorens-Cortes C. By interacting with the C-terminal Phe of apelin, Phe255 and Trp259 in helix VI of the apelin receptor are critical for internalization. J Biol Chem. 2010; 285:32627–32637. [PubMed: 20675385]
18. Iturrioz X, Alvear-Perez R, De Mota N, Franchet C, Guillier F, Leroux V, Dabire H, Le Jouan M, Chabane H, Gerbier R, et al. Identification and pharmacological properties of E339-3D6, the first nonpeptidic apelin receptor agonist. FASEB J. 2010; 24:1506–1517. [PubMed: 20040517]
19. Margathe JF, Iturrioz X, Regenass P, Karpenko IA, Humbert N, de Rocquigny H, Hibert M, Llorens-Cortes C, Bonnet D. Convenient access to fluorescent probes by chemoselective acylation of hydrazinopeptides: Application to the synthesis of the first far-red ligand for apelin receptor imaging. Chem Eur J. 2016; 22:1399–1405. [PubMed: 26682530]
20. Fournel A, Drougard A, Duparc T, Marlin A, Brierley SM, Castro J, Le-Gonidec S, Masri B, Colom A, Lucas A, et al. Apelin targets gut contraction to control glucose metabolism via the brain. Gut. 2017; 66:258–269. [PubMed: 26565000]

21. Ham JS. A new electronic state in benzene. J Chem Phys. 1953; 21:756–758.
22. Nakajima A. Solvent effect on the vibrational structures of the fluorescence and absorption spectra of pyrene. Bull Chem Soc Jpn. 1971; 44:3272–3277.
23. Dong DC, Winnik MA. The Py scale of solvent polarities. Solvent effects on the vibronic fine structure of pyrene fluorescence and emperical correlations with E_T and Y values. Photochem Photobiol. 1982; 35:17–21.
24. Förster T. Excimers. Angew Chem Int Ed. 1969; 8:333–343.
25. Wu P, Brand L. Resonance energy transfer: Methods and applications. Anal Biochem. 1994; 218:1–13. [PubMed: 8053542]
26. Langelaan DN, Reddy T, Banks AW, Dellaire G, Dupre DJ, Rainey JK. Structural features of the apelin receptor N-terminal tail and first transmembrane segment implicated in ligand binding and receptor trafficking. Biochim Biophys Acta. 2013; 1828:1471–1483. [PubMed: 23438363]
27. Langelaan DN, Bebbington EM, Reddy T, Rainey JK. Structural insight into G-protein coupled receptor binding by apelin. Biochemistry. 2009; 48:537–548. [PubMed: 19123778]
28. Johnson, I., Spence, M., editors. The Molecular Probes Handbook—A Guide to Fluorescent Probes and Labeling Technologies. 11. Life Technologies; Eugene, OR: 2010. p. 120
29. Gallea JI, Celej MS. Structural insights into amyloid oligomers of the Parkinson disease-related protein α-synuclein. J Biol Chem. 2014; 289:26733–26742. [PubMed: 25143382]
30. Panda D, Bhattacharyya B. Excimer fluorescence of pyrene-maleimide-labeled tubulin. Eur J Biochem. 1992; 204:783–787. [PubMed: 1541290]
31. Wu CW, Yarbrough LR. N-(1-pyrene)maleimide: A fluorescent cross-linking reagent. Biochemistry. 1976; 15:2863–2868. [PubMed: 7290]
32. Paul BC, Islam SS, Ismail K. Effect of acetate and propionate co-ions on the micellization of sodium dodecyl sulfate in water. J Phys Chem B. 1998; 102:7807–7812.
33. Stafford RE, Fanni T, Dennis EA. Interfacial properties and critical micelle concentration of lysophospholipids. Biochemistry. 1989; 28:5113–5120. [PubMed: 2669968]
34. Malliaris A, Le Moigne J, Sturm J, Zana R. Temperature dependence of the micelle aggregation number and rate of intramicellar excimer formation in aqueous surfactant solutions. J Phys Chem. 1985; 89:2709–2713.
35. Lipfert J, Columbus L, Chu VB, Lesley SA, Doniach S. Size and shape of detergent micelles determined by small-angle X-ray scattering. J Phys Chem B. 2007; 111:12427–12438. [PubMed: 17924686]
36. Chou JJ, Baber JL, Bax A. Characterization of phospholipid mixed micelles by translational diffusion. J Biomol NMR. 2004; 29:299–308. [PubMed: 15213428]
37. Bains G, Patel AB, Narayanaswami V. Pyrene: A probe to study protein conformation and conformational changes. Molecules. 2011; 16:7909–7935. [PubMed: 22143550]
38. Piñeiro L, Novo M, Al-Soufi W. Fluorescence emission of pyrene in surfactant solutions. Adv Colloid Interface Sci. 2015; 215:1–12. [PubMed: 25466688]
39. Kalyanasundaram K, Thomas JK. Environmental effects on vibronic band intensities in pyrene monomer fluorescence and their application in studies of micellar systems. J Am Chem Soc. 1977; 99:2039–2044.
40. Lide, DR., editor. CRC Handbook of Chemistry and Physics. 89. CRC Press; Boca Raton, FL: 2008.
41. Lianos P, Georghiou S. Solute-solvent interaction and its effect on the vibronic and vibrational structure of pyrene spectra. Photochem Photobiol. 1979; 30:355–362.
42. Arrais D, Martins J. Bilayer polarity and its thermal dependency in the l(o) and l(d) phases of binary phosphatidylcholine/cholesterol mixtures. Biochim Biophys Acta. 2007; 1768:2914–2922. [PubMed: 17976527]
43. Behera K, Pandey S. Modulating properties of aqueous sodium dodecyl sulfate by adding hydrophobic ionic liquid. J Colloid Interface Sci. 2007; 316:803–814. [PubMed: 17719598]
44. Hutchison, GR., Lambrecht, DS., Gupta, R., Rogan, J. Entry 2-(Trimethylammonio)Ethyl Dodecyl Phosphate. Pitt Quantum Repository, Department of Chemsitry, University of Pittsburgh; http://pqr.pitt.edu/mol/QBHFVMDLPTZDOI-UHFFFAOYSA-N [accessed April 11, 2017]

45. Stewart JJP. Optimization of parameters for semiempirical methods V: Modification of NDDO approximations and application to 70 elements. J Mol Model. 2007; 13:1173–1213. [PubMed: 17828561]

46. Hutchison, GR., Lambrecht, DS., Gupta, R., Rogan, J. Entry Sodium Lauryl Sulfate. Pitt Quantum Repository, Department of Chemsitry, University of Pittsburgh; http://pqr.pitt.edu/mol/DBMJMQXJHONAFJ-UHFFFAOYSA-M [accessed April 11, 2017]

47. Hutchison, GR., Lambrecht, DS., Gupta, R., Rogan, J. Entry [(1R)-1-[[[(2S)-2,3-Dihydroxypropoxy]-hydroxy-phosphoryl]oxymethyl]-2-hexadecanoyloxy-ethyl] (z)-octadec-11-enoate. Pitt Quantum Repository, Department of Chemsitry, University of Pittsburgh; http://pqr.pitt.edu/mol/ADYWCMPUNIVOEA-GPJPVTGXSA-N [accessed April 11, 2017]

48. Long JA, Rankin BM, Ben-Amotz D. Micelle structure and hydrophobic hydration. J Am Chem Soc. 2015; 137:10809–10815. [PubMed: 26222042]

49. Tamamizu-Kato S, Kosaraju MG, Kato H, Raussens V, Ruysschaert JM, Narayanaswami V. Calcium-triggered membrane interaction of the α-synuclein acidic tail. Biochemistry. 2006; 45:10947–10956. [PubMed: 16953580]

50. Zhou N, Zhang X, Fan X, Argyris E, Fang J, Acheampong E, DuBois GC, Pomerantz RJ. The N-terminal domain of APJ, a CNS-based coreceptor for HIV-1, is essential for its receptor function and coreceptor activity. Virology. 2003; 317:84–94. [PubMed: 14675627]

51. Haney EF, Lau F, Vogel HJ. Solution structures and model membrane interactions of lactoferrampin, an antimicrobial peptide derived from bovine lactoferrin. Biochim Biophys Acta. 2007; 1768:2355–2364. [PubMed: 17560539]

52. Kim JE, Arjara G, Richards JH, Gray HB, Winkler JR. Probing folded and unfolded states of outer membrane protein a with steady-state and time-resolved tryptophan fluorescence. J Phys Chem B. 2006; 110:17656–17662. [PubMed: 16942111]

53. le Maire M, Champeil P, Moller JV. Interaction of membrane proteins and lipids with solubilizing detergents. Biochim Biophys Acta. 2000; 1508:86–111. [PubMed: 11090820]

54. Chen J, Flaugh SL, Callis PR, King J. Mechanism of the highly efficient quenching of tryptophan fluorescence in human γD-crystallin. Biochemistry. 2006; 45:11552–11563. [PubMed: 16981715]

55. Oliver RC, Lipfert J, Fox DA, Lo RH, Doniach S, Columbus L. Dependence of micelle size and shape on detergent alkyl chain length and head group. PLoS One. 2013; 8:e62488. [PubMed: 23667481]

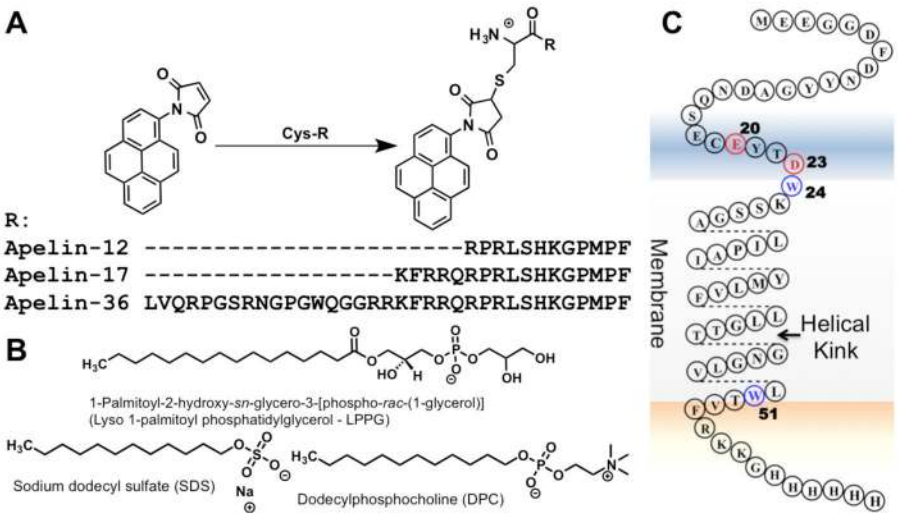

Figure 1.

Depiction of the (A) three pyrene-maleimide-Cys apelin conjugates employed herein (using one letter amino acid codes for compactness of apelin description); (B) the three surfactants employed for peptide-micelle interaction studies; and, (C) the AR55 protein construct (residues 1–55 of the apelin receptor (AR); topology based upon NMR structural studies and molecular dynamics simulations[26]) employed for pyrene-tryptophan FRET studies.

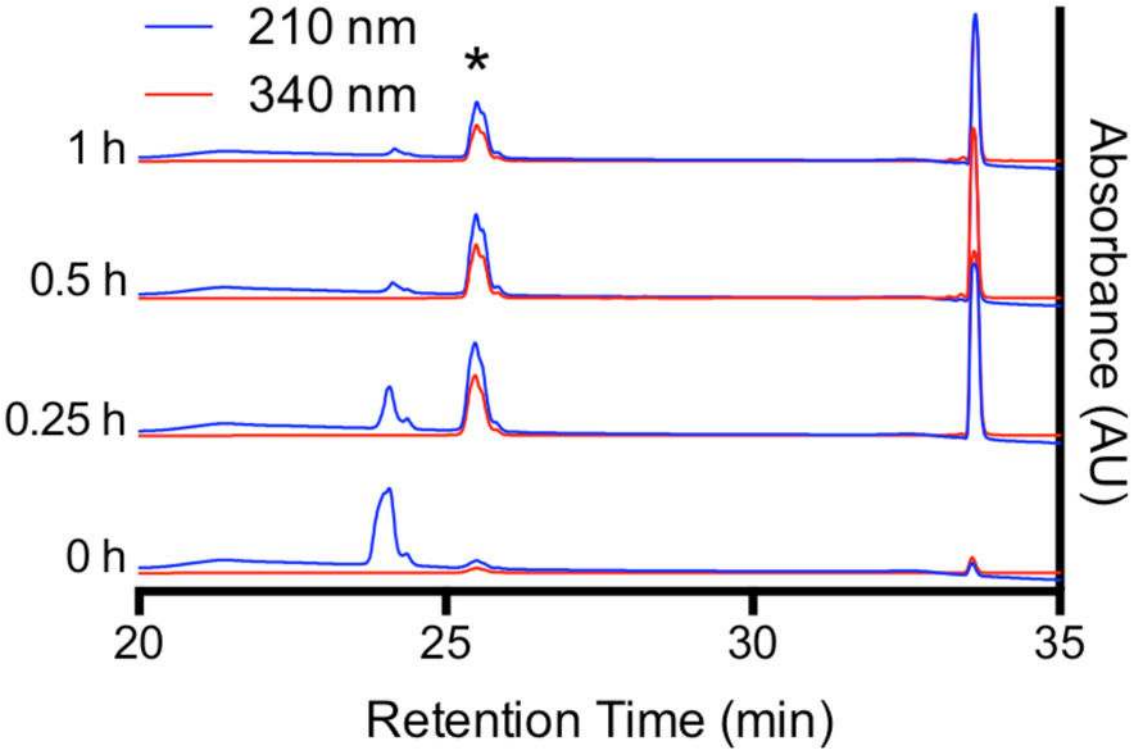

Figure 2.

RP-HPLC following pyrene maleimide conjugation to Cys-apelin-12 (eluent peak denoted by asterisk corresponds to Py-Cys-apelin-12, as confirmed by ESI-MS - deconvoluted mass 1822.8 Da vs. 1821.86 Da expected monoisotopic mass).

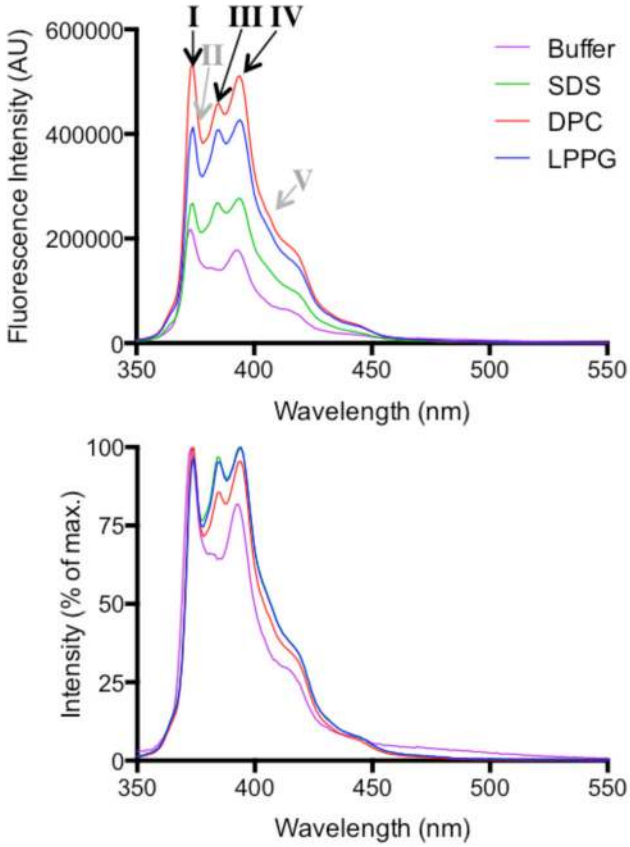

Figure 3.

Steady-state fluorescence emission spectra (excitation at 340 nm; normalized in lower panel to intensity of band I in given condition) of pyrene (1 μM with 100 mM of surfactant added). Bands I-V (colored grey for the less distinct bands II and V) are labeled.

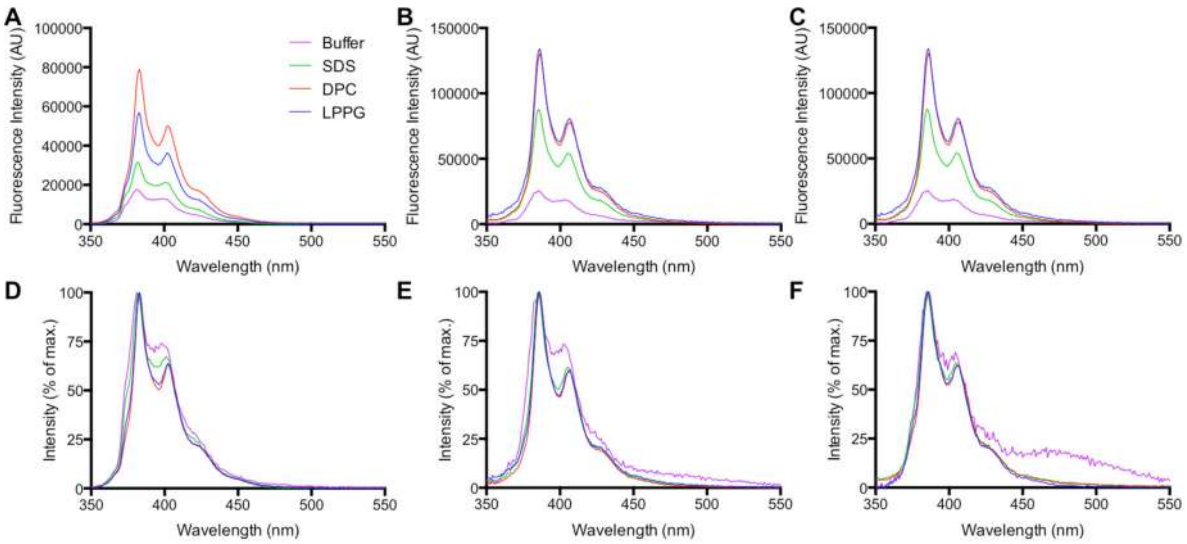

Figure 4.

Steady-state fluorescence emission spectra (excitation at 340 nm) of Py-Cys-apelin-12 (A; normalized in D), Py-Cys-apelin-17 (B; normalized in E), and Py-Cys-apelin-36 (C; normalized in F). All samples contained 1 μM peptide conjugate and, where appropriate, 100 mM surfactant; normalization was with respect to intensity of band I in given condition.

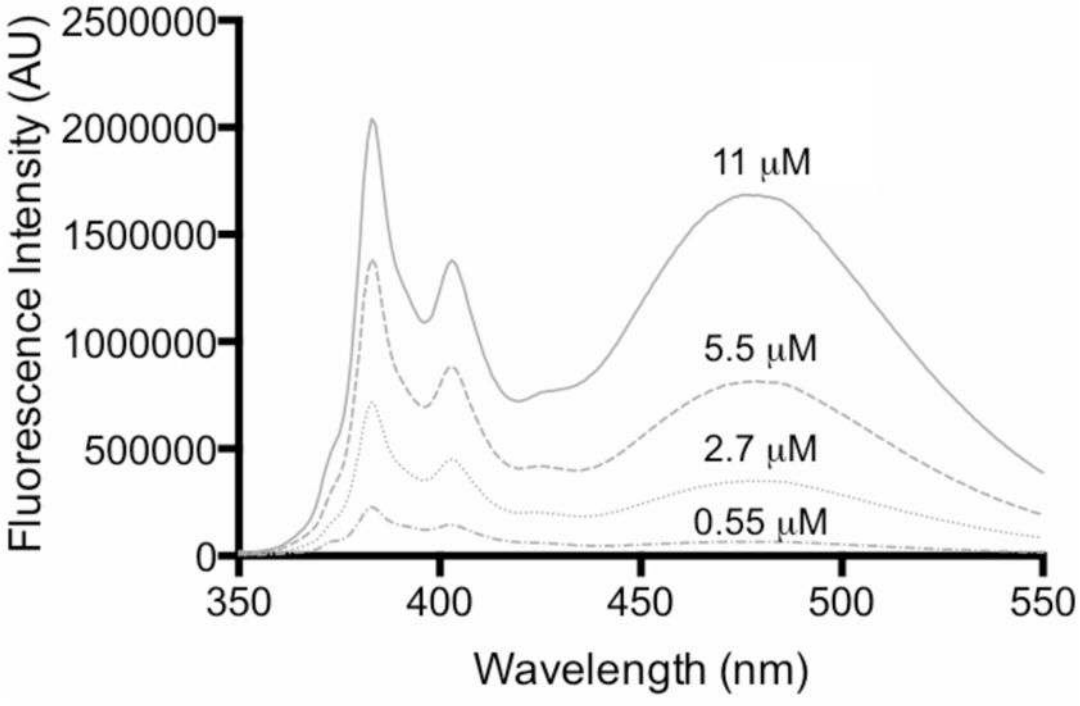

Figure 5.
Steady-state fluorescence emission spectra (excitation at 340 nm) of Py-Cys-apelin-12 at indicated concentration (containing sub-CMC, 1 mM, SDS).

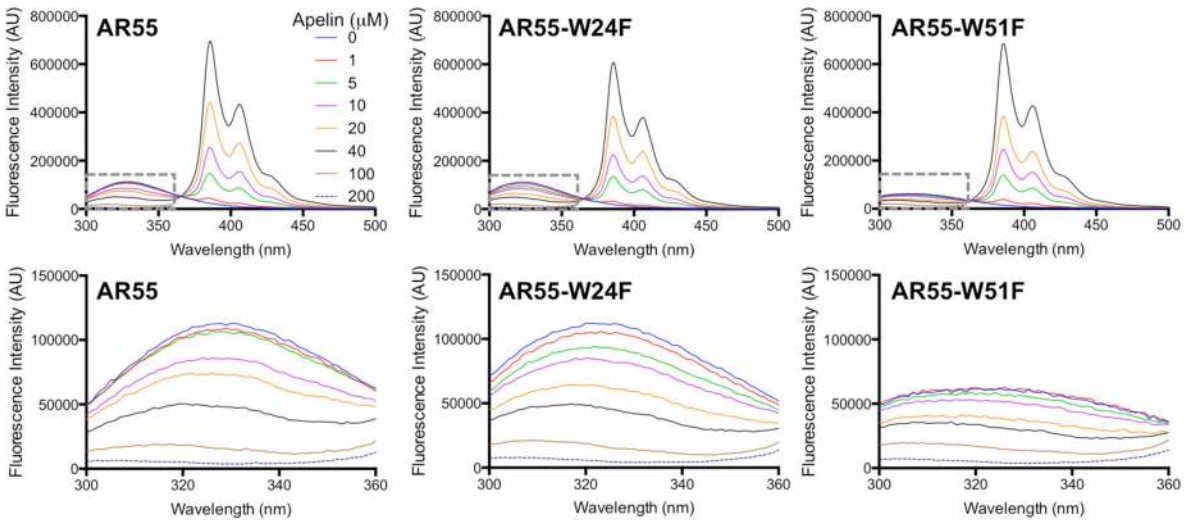

Figure 6.

Steady-state fluorescence emission spectra (excitation at 295 nm) of indicated AR55 construct (20 μM in 3.5 mM LPPG) titrated with Py-Cys-apelin-17. The dashed grey boxes (the tryptophan emission region) in the top row of spectra are expanded below each spectrum.

Table 1

Band I emission maximum (nm) and, correspondingly, band III attribution (nm) in given condition.

	Buffer		SDS		DPC		LPPG	
	I	III	I	III	I	III	I	III
Pyrene	373	383	374	384	374	384	374	384
Py-Cys-apelin-12	381	392	382	392	383	393	383	393
Py-Cys-apelin-17	385	395	385	395	386	396	386	396
Py-Cys-apelin-36	386	396	385	395	386	396	386	396

Table 2

Py values (eq. 1, mean±SEM, triplicate experiments) for a given sample in the indicated condition.

	Buffer	**SDS**	**DPC**	**LPPG**
Pyrene	1.50±0.060	0.99±0.036	1.16±0.055	1.00±0.048
Py-Cys-apelin-12	1.38±0.025	1.59±0.002	1.76±0.013	1.73±0.039
Py-Cys-apelin-17	1.45±0.007	1.79±0.034	1.78±0.027	1.85±0.054
Py-Cys-apelin-36	1.45±0.044	1.64±0.039	1.79±0.028	1.75±0.010

Table 3

FRET efficiency (E, eq. 2; based upon Trp quenching), pyrene *Py* value (eq. 1), and wavelength of tryptophan emission maximum (l_{max}) for given AR55 construct at 20 μM in LPPG micelles titrated with Py-Cys-apelin-17. (All values are averages from triplicates.)

	AR55			**AR55-W24F**			**AR55-W51F**		
[Apelin] (μM)	**E**	***Py***	**λ_{max} (nm)**	**E**	***Py***	**λ_{max} (nm)**	**E**	***Py***	**λ_{max} (nm)**
0	0	-	321	0	-	320	0	-	321
1	0.032	1.71	329	0.062	1.66	323	0.0022	1.74	320
5	0.057	1.87	326	0.17	1.85	322	0.045	1.88	319
10	0.24	1.89	324	0.25	1.88	320	0.13	1.90	316
20	0.36	1.89	326	0.43	1.90	318	0.34	1.89	317
40	0.55	1.90	320	0.56	1.91	317	0.42	1.90	315
100	0.83	ND	318	0.81	ND	309	0.68	ND	309
200	0.94	ND	ND	0.93	ND	ND	0.88	ND	ND
Plateau	0.94	-	-	0.89	-	-	0.88	-	-